Atmos. Chem. Phys. Discuss., 10, 20887–20920, 2010
www.atmos-chem-phys-discuss.net/10/20887/2010/
doi:10.5194/acpd-10-20887-2010

Atmospheric Chemistry and Physics Discussions

The Bihar Pollution Pool as observed from MOPITT (version 4), CALIPSO (version 3) and tropospheric ozone residual data

J. Kar[1], **M. N. Deeter**[2], **J. Fishman**[3], **Z. Liu**[3,4], **A. Omar**[3], **J. K. Creilson**[1,3], **C. R. Trepte**[3], **M. A. Vaughan**[3], **and D. M. Winker**[3]

[1]Science Systems and Applications Inc., Hampton, VA, 23666, USA
[2]National Center for Atmospheric Research, Boulder, CO, USA
[3]NASA Langley Research Center, Hampton, VA, 23681, USA
[4]National Institute of Aerospace, Hampton, VA, 23666, USA

Received: 19 August 2010 – Accepted: 29 August 2010 – Published: 1 September 2010

Correspondence to: J. Kar (jayanta.kar@nasa.gov)

Published by Copernicus Publications on behalf of the European Geosciences Union.

Abstract

The Bihar pollution pool is a large wintertime increase in pollutants over the eastern parts of the Indo Gangetic basin. We use improved carbon monoxide (CO) retrievals from the recent Measurements of Pollution in the Troposphere (MOPITT) version 4 data along with the aerosol data from the latest version 3 of the Cloud-Aerosol Lidar and Infrared Pathfinder Satellite Observations (CALIPSO) lidar instrument and the tropospheric ozone residual products from the Total Ozone Mapping Spectrometer (TOMS)/Solar Backscattered Ultraviolet (SBUV) and Ozone Monitoring Instrument (OMI)/Microwave Limb Sounder (MLS) database to characterize this pollution pool. The feature is seen primarily in the lower troposphere from about November to February with strong concomitant increase in CO, aerosol optical depth and tropospheric ozone columns. The height resolved aerosol data from CALIPSO confirm the trapping of the pollution pool at the lowest altitudes. The observations indicate that MOPITT can capture this low altitude phenomenon even in winter conditions as indicated by the averaging kernels.

1 Introduction

The Indo Gangetic basin (IGB) straddling the north eastern parts of India near the foot hills of the Himalayas is one of the most densely populated regions on the globe with consequent large anthropogenic emissions. In particular the use of traditional biofuels in the rural areas along the basin leads to strong emissions of various pollutants. It is also a region with many power plants and industries and the recent economic growth of India has led to significant increase in industrial emissions (Ghude et al., 2008). As such, the high level of pollution in this region has been the subject of several studies over the last few years using data both from ground based and space based observations as well as models (Jethva et al., 2005; Tripathi et al., 2006; Gautam et al., 2007, 2009; Beig and Ali, 2006; Roy et al., 2008; Kar et al., 2008, 2009; Clarisse et al., 2009).

ACPD

10, 20887–20920, 2010

Fishman et al. (2003) had found high tropospheric ozone residual (TOR) along this basin all through the year. The large sources of emission along the basin has implications also for regional pollution, as deep convection during the monsoon months can efficiently lift the pollution to the upper troposphere which can then be transported westward along the southern edge of the Tibetan anticyclonic circulation. The latter has been observed as the Asian summer monsoon plume in satellite measurements of various trace species like CO, CH_4, ozone etc. and has been modeled as well (Kar et al., 2004; Li et al., 2005; Park et al., 2007; Lawrence et al., 2003; Lawrence and Lelieveld, 2010; Xiong et al., 2009).

In the winter months the IGB is often enveloped by thick fog and haze (Gautam et al., 2007). A striking observation from the Multi-angle Imaging SpectroRadiometer (MISR) instrument aboard Terra was the high aerosol optical depths in the winter months over the eastern parts of the IGB, the so-called Bihar pollution pool (extending over the provinces of Bihar and West Bengal in India as well as over Bangladesh), which is caused by the trapped pollution owing to strong localized subsidence and low wind speeds during this season (Di Girolamo et al., 2004). As pointed out by Di Girolamo et al. (2004), this observation has strong implications for the large population residing in this area and thus calls for further work. Kar et al. (2008) using the CO retrievals from MOPITT (version 3 data) found a corresponding pool of high CO mixing ratios at 850 hPa level in the same area in winter. However, as noted by Kar et al. (2008), in all of version 3 MOPITT data, there was a persistent wide swath of data drop out along much of the IGB which did not allow the feature to be studied fully. The reason for this data drop out was not clear at that time. A much improved version 4 of MOPITT data has now become available (Deeter et al., 2010). As mentioned by Deeter et al. (2010), the use of the original training set in the MOPITT algorithm led to non-convergence of retrievals in regions with very large CO mixing ratios. A revised training set now leads to many more convergent retrievals. In fact in version 4 data the large data drop out region along the IGB is no longer visible, possibly from these added retrievals in this highly polluted region. In this paper we therefore study the Bihar pollution pool using

ACPD
10, 20887–20920, 2010

this new MOPITT CO dataset. While the phenomenon was initially noted in the MISR aerosol optical depth data, new height resolved aerosol data from CALIPSO have now become available which should provide further insight into the vertical distribution of the feature. We therefore use these aerosol data from the CALIPSO lidar instrument as also the tropospheric ozone columns from the TOR and TCO databases to further characterize this winter time phenomenon over the eastern parts of the IGB.

2 Data

We use CO retrievals from the MOPITT instrument on board Terra (Drummond, 1992; Drummond et al., 2010). MOPITT has been providing global measurements of CO profiles since March 2000 using gas correlation radiometry and the data have been used widely to study the global distribution of CO and various transport phenomena in the troposphere. Recently a new version of the data (version 4) has been released which differs from the version 3 in many respects (Deeter et al., 2010). Primarily, improved retrievals result from a more realistic a priori, essential for the optimal estimation technique employed for the CO retrieval algorithm. Specifically a monthly mean climatology obtained from the Model for Ozone and Related chemical Tracers, version 4 (MOZART-4) chemical transport model interpolated to the location and day of the MOPITT retrievals is used in version 4 rather than the uniform a priori profile employed in version 3 (for details see Deeter et al., 2010). Further, the state vector is represented in the form of log(vmr) rather than as vmr (volume mixing ratio) as was done in version 3 and the training set for the radiative transfer code was expanded by adding a set of highly-polluted profiles obtained by scaling each of the original CO profiles by a factor of two. The latter leads to valid retrievals over the locations with high CO sources, where the version 3 algorithm resulted in significant data drop outs (Deeter et al., 2010). We use the level 3 gridded monthly mean profiles (at 9 uniform pressure levels from 900 hPa to 100 hpa) from the version 4 MOPITT data. We also use aerosol products retrieved by the CALIPSO lidar instrument which has been providing height resolved

ACPD
10, 20887–20920, 2010

aerosol information globally since 2006 (Winker et al., 2009). CALIPSO provides total attenuated backscatter profiles at 532 nm and 1064 nm and a perpendicular polarization component for 532 nm. A new version (V.3.01) of CALIPSO data has just been released with significant improvements in the cloud-aerosol screening module as well as extended profiles below layers with strong attenuation and also provides the column integrated optical depth information for the first time. The depolarization ratio from the 532 nm channel provides useful information about the shape of the aerosol particles while the color ratio provides information on the size of the aerosol particles (Z. Liu et al., 2008). We use the 5 km aerosol layer products from CALIPSO data. Further we make use of the tropospheric column ozone data from two products. In the empirically corrected tropospheric ozone residuals (TOR), the stratospheric column ozone (SCO) is determined by an empirical correction applied to the tropospheric profile as retrieved by the SBUV measurements and subsequently the resulting SCO is subtracted from the TOMS total column measurements (Fishman and Balok, 1999). Monthly mean fields of TOR are available and encompass the time period from 1979–2005 with missing data for the years 1994–1996. We also use the tropospheric column ozone (TCO) database derived by Ziemke et al. (2006) from the OMI and MLS instruments after cross calibrating the MLS SCO with OMI SCO obtained by the convective cloud differential method. These data have similar spatial resolution as the TOR data ($1^{\circ} \times 1.25^{\circ}$) and are available from October 2004 onwards as monthly means. We have also used aerosol optical depth (AOD) data from the AERONET station at Kanpur. Only the quality assured level 2 version 2 data were used for the years 2006–2009. We have also used the pressure tendency (omega) data from the National Centers for Environmental Prediction (NCEP) reanalyses (Kalnay et al., 1996).

ACPD
10, 20887–20920, 2010

3 Results

3.1 Bihar Pollution Pool in MOPITT CO (version 4) data

Figure 1 shows a comparison of monthly mean profiles for December 2005 within the IGB area from version 3 (V3) and version 4 (V4) MOPITT data for 2 grid cells centered at 24.5° N, 84.5° E and 26.5° N, 80.5° E. Also shown are the corresponding a priori profiles from the two versions of the data (as dashed lines). The constant a priori profile in V3 differs significantly from the V4 a priori profiles below 500 hPa. The V4 mean profile at 26.5° N, 80.5° E was computed from 37 CO retrievals which were not available in V3 data and thus did not have a corresponding mean V3 profile for this grid cell. The large value of ∼260 ppbv at 900 hPa indicates that these valid retrievals in V4 may have come about because of the revised training set as mentioned above, since the cloud clearing algorithm is the same in both the versions (Deeter et al., 2010). The V4 mean profile at 24.5° N, 84.5° E, on the other hand had a corresponding monthly mean V3 profile with the same number of profiles in both the versions. Significant differences can be seen in the middle and lower tropospheric mixing ratios once again with much higher values in the lowest levels in version 4. The added retrievals over the IGB area now make it possible to clearly delineate the Bihar pollution pool (BPP) during the winter months. This is shown in Fig. 2 in the spatial distribution of CO at 900 hPa between the months of November 2006 to February 2007. We have used the dayside data (with mean uncertainty less than 50%) only, as these have typically higher vertical resolution than the nightside data (Deeter et al., 2010). As can be seen, very high values of CO mixing ratios at 900 hPa develop over a large area in the north eastern parts of the IGB reaching ∼300 ppbv in December and January (∼20° N–27° N, 80° E–90° E). In absence of any significant biomass burning in this area in winter, these enhanced CO levels are generated by anthropogenic activities. The high CO values seen over South East Asia (eastward of ∼90° E) in February are likely due to the seasonal biomass burning as evidenced by the large number of hotspots in Along Track Scanning Radiometer (ATSR) maps over this area (not shown). Similar evolution

ACPD
10, 20887–20920, 2010

of the feature in CO distributions at 900 hPa was also seen for other years, implying that it is a robust wintertime feature that was first seen in the MISR aerosol optical depth data (Di Girolamo et al., 2004) and was also detected in the partially available CO version 3 data from MOPITT over the region in December for various years (Kar et al., 2008). The fact that this feature was detected in the MOPITT version 3 data (at 850 hPa) as well (Kar et al., 2008), which employed a single constant a priori profile, implies this is indeed a robust result and may not be simply attributed to the variable a priori employed in the version 4 data, although the a priori distributions at 900 hPa have similarities with the retrieved CO at 900 hPa (not shown).

The detection of the BPP in MOPITT CO data has to be consistent with the sensitivity of MOPITT retrievals. Figure 3a (top panel) shows the monthly mean averaging kernels from MOPITT V4 data at 24.5° N, 84.5° E for all the 10 levels including the surface level for the month of December 2006. The V4 averaging kernels represent the sensitivity of the MOPITT retrievals (log(vmr) value retrieved at one level) to log(vmr) perturbations in the true profile at another level. The averaging kernels provide a measure of the vertical resolution of the retrievals (Deeter et al., 2004, 2007). The V4 averaging kernels as seen in Fig. 3a indicate significant information content in the MOPITT V4 retrievals over this area even in December with about two pieces of information. As can be seen, all the lower level kernels are peaking at 900 hPa level, thus implying significant information coming from the lowest levels of the atmosphere. In particular the 900 hPa kernel is sharply peaking at the same level with highest value of ∼0.23. The sharp decrease in all the kernels from 900 hPa to the surface is due to an artifact of the pressure-grid employed – the thickness of the surface layer (and thus the absorber amount perturbation) is smaller compared to those of the levels higher up except the highest one at 100 hPa (for details of this effect see Deeter et al., 2007). Figure 3b shows the monthly mean 900 hPa kernels from November 2006 to February 2007. For all months, the 900 hPa kernels peak at 800–900 hPa level.

Figure 4a shows a height latitude distribution from version 4 MOPITT CO profiles averaged over (85° E–90° E) for December 2006, while Fig. 4b shows the corresponding

ACPD
10, 20887–20920, 2010

height latitude distribution of the pressure tendency (omega = dp/dt in Pa s^{-1}) taken from the NCEP reanalyses. While oceanic convection (negative omega) can be seen between 5° N–15° N with signatures of lifted CO into the middle troposphere, strong accumulation of pollution at the lowest altitudes occurs over the Indian landmass, consistent with the strong subsidence (positive omega) seen over the BPP region (~21° N–27° N). As noted by Di Girolamo et al. (2004) and Dey and Di Girolamo (2010), the combination of strong subsidence and low wind speeds (<5 m s^{-1}) inhibit venting of this pollution above the boundary layer.

A decade of MOPITT observations makes it possible to study the BPP feature over time. Figure 5 shows a plot of the time series of the difference between the mean CO at 900 hPa level within the BPP area (~20° N–27° N, 80° E–90° E) and that for similar latitude range over the western parts of the country (~20° N–27° N, 65° E–80° E). The difference generally increases sharply during the fall through winter months and tends to decrease during the summer months, although large scale data drop outs during the monsoon months might be biasing the results somewhat. Also the high values often persist up to March and April, possibly because of the influence of the biomass burning in the South East Asia and within India towards the eastern edge of BPP.

3.2 Bihar Pollution Pool in CALIPSO (version 3) data

Further direct evidence of the low altitude BPP phenomenon comes from the CALIPSO height resolved aerosol data. Figure 6a shows the total attenuated backscatter at 532 nm on 1 January 2007 along a transect crossing the BPP area. The transect is shown in the inset of the bottom panel. Strong aerosol layers (red-grayish features) can be seen over the area from ~20° N to the foot hills of the Himalayas essentially confined below ~2 km altitude range. Earlier, Jethva et al. (2005) had used the low values of the TOMS absorbing aerosol index over the IGB in winter to infer that the winter time aerosols are trapped within the boundary layer. The vertical feature mask shown in Fig. 6b indicates primarily aerosol layers over the land from 20° N to ~28° N

Discussion Paper | Discussion Paper | Discussion Paper | Discussion Paper |

ACPD

10, 20887–20920, 2010

The Bihar Pollution Pool as observed from MOPITT, CALIPSO and TOR

J. Kar et al.

up to the foot hills of the Himalayas. In the Version 3 CALIPSO data released very recently, the aerosol subtypes are now directly available in the level 1 browse images. Figure 6c shows the corresponding subtype information for this scene. In the BPP area (~20° N–28° N) several different aerosol subtypes can be discerned with polluted continental and polluted dust at the lowest levels overlain with dust and smoke.

In order to characterize the aerosol environment in the BPP area we use the 5 km aerosol layer product from CALIPSO V3 data. Figure 7 shows the altitude distributions of the top of the layers (above surface level) in the different seasons for the year 2007. All layers between surface and 6 km with Cloud Aerosol Discrimination (CAD) score of −100 only, were included. A CAD score of −100 indicates that the layer has been identified as an aerosol layer with complete confidence (Liu et al., 2009, 2010). Significant seasonal changes in the altitude distribution can be seen. The winter (December 2006 through February 2007) distribution is clearly different from the other seasons with maximum number of aerosol layers with the bulk of them having top altitudes within 2–3 km. In contrast a significant number of layers in spring have top altitudes in excess of 3 km. These layers are likely the dust layers transported into the BPP region from the western parts of the sub-continent. In summer the number of layers drops drastically, indicating the influence of the monsoon.

The spatial and optical properties of the aerosols along with other ancillary data are used to obtain the aerosol subtypes in the CALIPSO algorithm (Omar et al., 2009). Figure 8 shows the seasonal variation of the dominant subtypes (as a fraction of the total number of layers) over the BPP (~ 20° N–27° N, 80° E–90° E) area during 2007. All layers with top altitudes below 6 km and CAD score of −100 have been used for this plot. While dust dominates during spring and early summer, polluted dust seems to dominate throughout the rest of the year with smaller contributions from polluted continental and smoke. While dust coming from the northwestern parts declines during the monsoon months, contribution from locally generated dust becomes important during the fall and winter months. This is consistent with the findings of Dey and Di Girolamo (2010), who attribute the low Angstrom exponent and slightly higher non-spherical

ACPD
10, 20887–20920, 2010

component of the AOD over the Eastern IGB in winter to high concentration of coarse dust particles from rural activities. Figure 9 shows the altitudes (top of layers above the surface) of these dominant subtypes taken along a longitude belt of 80° E–90° E during the winter months (December 2006–February 2007). Once again, the low altitude aerosol layers (below 30° N) are primarily composed of polluted dust and polluted continental types with some smoke and dust layers mixed with these.

The aerosol subtype algorithm in CALIPSO retrieval scheme primarily provides an estimate of the lidar ratio (i.e., the aerosol extinction-to-backscatter ratio) used subsequently in the extinction algorithm (Omar et al., 2009). In view of the significant improvements in the version 3 data from extension of the aerosol profiles below optically thick layers (Vaughan et al., 2010) and cloud-aerosol discrimination algorithms (Liu et al., 2010), the layer optical depths as well as the column integrated optical depths (which is a new product in V3) should provide valuable information about the BPP feature. Figure 10 shows the layer optical depths in the winter of 2006–2007 obtained from the CALIPSO extinction retrievals at 532 nm over the BPP area. Only those layers with CAD score of −100, estimated uncertainty in the layer optical depth less than the optical depth and extinction QC value of either 0 (solutions with final lidar ratio unchanged) or 1 (constrained retrievals) was used. Most layers have optical depths within about 0.6 but some can go up to 1.0 or more.

Figure 11 shows a comparison between the monthly mean column aerosol optical depths (AOD) obtained from the AERONET station at Kanpur and CALIPSO. Kanpur (26.5° N, 80.4° E) is located near the northern edge of the BPP. Only the quality assured level 2 version 2 data from AERONET database have been used here for the time period June 2006 to December 2009. We used a coincidence box of 0.5 × 0.5 deg in latitude and longitude around the location of Kanpur and used the daytime 532 nm column AOD data from CALIPSO for this comparison. The CALIPSO AOD data were filtered using two criteria: (a) the column AOD uncertainty less than the column AOD value and (b) the extinction QC value of 0 or 1 for each of the layers within a particular column. The AERONET monthly mean data at 500 nm were interpolated to 532 nm

ACPD
10, 20887–20920, 2010

using the Angstrom exponent in the range 440–675 nm. There were a total of 32 points available for this comparison. The comparison in Fig. 11 shows a reasonable agreement between the two data sets (linear correlation coefficient ∼0.5) with CALIPSO retrieving lower optical depths more often than not. It should be mentioned that we have not filtered the CALIPSO data for presence of clouds because of the few data points available for comparison.

Figure 12 shows the spatial distribution of AOD at 532 nm from CALIPSO V3 over India between November 2006 and February 2007. Only night time data were used because of generally low SNR in the dayside CALIPSO data because of the solar influence. Once again, the AOD data were filtered using the two criteria stated in the last paragraph. The data were binned in 3.636° in latitude and 3.06° in longitude, which ensures uniform sampling within each grid cell. Because of the sparse sampling of CALIPSO, the fine details of these plots should be viewed with some caution. However, it is clear that the spatial pattern is generally similar to the CO distribution from MOPITT, with a plume of high AOD (∼0.6) over the BPP area (20° N–27° N, 80° E–90° E). The AOD values are quite similar to the maximum AOD values of about 0.6 reported over this region from the MISR instrument at 558 nm in winter as well as from Moderate Resolution Imaging SpectroRadiometer (MODIS) at 550 nm in this area (Di Girolamo et al., 2004; Jethva et al., 2005). CALIPSO data were not available from 5–18 December 2006. The BPP plume is well delineated in November through January and decreases in strength in February. This result attests to the fidelity of the CALIPSO AOD retrievals over this highly polluted area. Once again, we used all data for this plot without filtering for clouds. However, we examined the effect of clouds by retaining only the cloud free data (cloud column optical depth = 0). While this led to data dropouts, it did not affect the main results. Figure 13 shows the inter annual variation of the feature in CALIPSO data for the month of December using the 4 years of data available. The BPP plume occurs every year with some inter annual variability. Once again this suggests that the BPP plume is a robust feature.

ACPD
10, 20887–20920, 2010

3.3 Bihar Pollution Pool in the tropospheric column ozone data

The large regional enhancement of CO and aerosol at low altitudes over the BPP area may have implications for ozone levels in the area. We examined the tropospheric column ozone over this area using both the TOR and TCO data. Figure 14 (top panel) shows an example of regionally enhanced TOR values over the BPP area in January 2006. Note the highest TOR values (~40 DU, 1 DU ≡ 2.69×10^{16} molecules per cm^2) occur essentially over the BPP area where CO is regionally strongly enhanced. Figure 14b (bottom panel) shows the corresponding plume as seen in the TCO distribution. The close similarity between the spatial distributions from two different tropospheric residual products lends credence to this feature in ozone and perhaps implies that the two products are capturing low altitude ozone produced from the enhanced levels of precursors like CO over this area at this time. The TOR values in 2006 were estimated by subtracting the SCO obtained from the Global Forecast System (GFS) model (which assimilates SBUV information) from the total ozone column retrieved by the OMI instrument. Thus the primary information on the troposphere is coming from the OMI instrument for both TOR and TCO for January 2006 and should be linked to the vertical sensitivity of the total ozone column retrievals from the OMI measurements. The latter has been quantified in terms of an "efficiency factor" and is reported in the level 2 data products of OMI at 11 levels corresponding to the mid points of the Umkehr layers (at 2.8, 7.9, 12.5, 17.0, 21.3, 25.8, 30.4, 35.2, 40.2, 45.5, 51.0 km) and represents the sensitivity of the total ozone column to perturbations in a particular layer. The value of the efficiency factor at the lowest level (2.8 km) averaged over 20° N–27° N, 80° E–90° E for January 2006 comes out to be about 0.5 and its spatial distribution shows regionally enhanced values of the efficiency factor along the IGB (not shown). Therefore it is possible that both TOR and TCO are capturing some of the enhancements of low altitude ozone in this area in winter. Both TOR (1979–2005) and TCO (2004–2008) climatologies show enhanced ozone over BPP during the winter (December, January and February) months (not shown). While both show regional enhancements of about

3–4 DUs, there are significant differences in absolute values and spatial patterns in the two maps. In TOR data, there is enhanced ozone along the entire Indo Gangetic basin, while the TCO distribution shows more localized enhancements covering the BPP area. The reason for these anomalies between TOR and TCO distributions is not clear but may have to do with the ways the SCOs are determined in the two methods. A more thorough analysis of this is beyond the scope of this work.

Given the level of pollution in this highly populated area, it is pertinent to explore the long term tropospheric ozone in the BPP area. This information is available from the nearly 25 years of TOR data from 1979 to 2006 (except for the years 1994–1996). Figure 15 shows the inter annual variation of TOR for the month of January over the BPP area. A modest inter annual variation can be seen with TOR varying by ~5 DU mostly. However, no significant overall trend can be discerned in the data. Also plotted in Fig. 15 are the corresponding monthly mean values of omega at the 850 hPa level from NCEP reanalyses. The positive omega values imply subsidence in all years which would tend to promote photochemistry (Fishman et al., 2005). Apart from the abundance of the precursors like CO and meteorology, the TOMS efficiency factors may also determine how much of the low level ozone will be captured by the TOR values in different months.

4 Conclusions

The extensive pollution along the eastern parts of the IGB during winter months has been studied using the improved version 4 CO data from MOPITT and the new version 3 height resolved aerosol data from CALIPSO as well as the tropospheric column ozone from 2 different data products. The new CO data show very high mixing ratios in the lower troposphere that primarily develop during November–February. Both the CO and aerosol data confirm the trapping of pollution at low altitudes by subsidence. Furthermore, the TOR and TCO residual ozone column data show similar spatial distribution of enhanced ozone over this area. The latter indicates that the TOR and

ACPD
10, 20887–20920, 2010

TCO data are capturing some of the ozone being produced locally by photochemistry from the precursors at low altitudes and thus implies their usefulness for monitoring air quality in highly polluted areas. Overall these new satellite data confirm very high anthropogenic pollution in the BPP area in winter and call for continual monitoring and mitigation strategies.

Acknowledgements. We are grateful to Jerry Ziemke for providing the tropospheric column ozone data through the NASA Goddard tropospheric ozone website. We thank Brent Holben and S. N. Tripathi for their efforts in establishing and maintaining the Kanpur AERONET site. JK thanks Jean-Paul Vernier for discussions and Ralph Kuehn for a useful suggestion on binning of CALIPSO data.

References

Beig, G. and Ali, K.: Behavior of boundary layer ozone and its precursors over a great alluvial plain of the world: Indo-Gangetic plains, Geophys. Res. Lett., 33, L24813, doi:10.1029/2006GL028352, 2006.

Clarisse, L., Clerbaux, C., Dentener, F., Hurtmans, D., and Coheur, P.-F.: Global ammonia observations derived from infrared satellite observations, Nat. Geosci., 2, 479–483, doi:10.1038/NGEO551, 2009.

Deeter, M. N., Emmons, L. K., Edwards, D. P., Gille, J. C., and Drummond, J. R.: Vertical resolution and information content of CO profiles retrieved by MOPITT, Geophys. Res. Lett., 31, L15112, doi:10.1029/GL020235, 2004.

Deeter, M. N., Edwards, D. P., Gille, J. C., and Drummond, J. R.: Sensitivity of MOPITT observations to carbon monoxide in the lower troposphere, J. Geophys. Res., 112, D24306, doi:10.1029/2007JD008929, 2007.

Deeter, M. N., Edwards, D. P., Gille, J. C., Emmons, L. K., Francis, G., Ho, S.-P., Mao, D., Masters, D., Worden, H., Drummond, J. R., and Novelli, P. C.: The MOPITT version 4 CO product: algorithm enhancements, validation and long-term stability, J. Geophys. Res., 115, D07036, doi:10.1029/2009JD013005, 2010.

Di Girolamo, L., Bond, T. C., Bramer, D., Diner, D. J., Fettinger, F., Kahn, R. A., Martonchik, J. V., Ramana, M. V., Ramanathan, V. and Rasch, P. J.: Analysis of multi-angle imaging

ACPD
10, 20887–20920, 2010

spectro-radiometer (MISR) aerosol optical depths over greater India during winter 2001–2004, Geophys. Res. Lett., 31, L23115, doi:10.1029/2004GL0211273, 2004.
Dey, S. and Di Girolamo, L.: A climatology of aerosol optical and microphysical properties over the Indian subcontinent from nine years (2000–2008) of Multiangle Imaging SpectroRadiometer (MISR) data, J. Geophys. Res., 115, D15204, doi:10.1029/2009JD013395, 2010.
Drummond, J. R.: Measurements of pollution in the troposphere, in: The Use of EOS for studies of Atmospheric Physics, edited by: Gille, J. C., and Visconti, G.: 77–101, North-Holland, Amsterdam, 1992.
Drummond, J. R., Zou, J., Nichitiu, F., Kar, J., Deschambaut, R. and Hackett, J.: A review of 9-year performance and operation of the MOPITT instrument, Adv. Space Res., 45, 760–774, doi:10.1016/j.asr.2009.11.019, 2010.
Fishman, J. and Balok, A. E.: Calculation of daily tropospheric ozone residuals using TOMS and empirically improved SBUV measurements: Application to an ozone pollution episode over the eastern United States, J. Geophys. Res., 104, 30319–30340, 1999.
Fishman, J., Wozniak, A. E., and Creilson, J. K.: Global distribution of tropospheric ozone from satellite measurements using the empirically corrected tropospheric ozone residual technique: Identification of the regional aspects of air pollution, Atmos. Chem. Phys., 3, 893–907, doi:10.5194/acp-3-893-2003, 2003.
Fishman, J., Creilson, J. K., Wozniak, A. E., and Crutzen, P. J.: Interannual variability of stratospheric and tropospheric ozone determined from satellite measurements, J. Geophys. Res., 110, D20306, doi:10.1029/2005JD005868, 2005.
Gautam, R., Hsu, N. C., Kafatos, M., and Tsay, S.-C.: Influences of winter haze on fog/low cloud cover over the Indo-Gangetic plains, J. Geophys. Res., 1112, D05207, doi:10.1029/2005JD007036, 2007.
Gautam, R., Liu, Z., Singh, R. P., and Hsu, N. C.: Two contrasting dust-dominant periods over India observed from MODIS and CALIPSO data, Geophys. Res. Lett., 36, L06813, doi:10.1029/2008GL036967, 2009.
Ghude, S., Fadnavis, S., Beig, G., Polade, S. D., and van der A, R. J.: Detection of surface emission hot spots, trends, and seasonal cycle from satellite-retrived NO_2 over India, J. Geophys. Res., 113, D20305, doi:10.1029/2007JD009615, 2008.
Jethva, H., Satheesh, S. K., and Srinivasan, J.: Seasonal variability of aerosols over the Indo-Gangetic plains, J. Geophys. Res., 110, D21204, doi:10.1029/2005JD005938, 2005.
Kalnay, E., Kanamitsu, M., Kistler, R., Collins, W., Deaven, D., Gandin, L., Iredell, M., Saha,

ACPD
10, 20887–20920, 2010

The Bihar Pollution Pool as observed from MOPITT, CALIPSO and TOR

J. Kar et al.

S., White, G., Woollen, J., Zhu, Y., Chelliah, M., Ebisuzaki, W., Higgins, W., Janowiak, J., Mo, K. C., Ropelewski, C., Wang,J., Leetmaa, A., Reynolds, R., Roy,J., and Joseph, D.: The NCEP/NCAR 40-Year Reanalysis Project, B. Am. Meteorol. Soc., 77(3), 437–471, 1996.

Kar, J., Bremer, H., Drummond, J. R., Rochon, Y. J., Jones, D. B. A., Nichitiu, F., Zou, J., Liu, J., Gille, J. C., Edwards, D. P., Deeter, M. N., Francis, G., Ziskin, D., and Warner, J.: Evidence of vertical transport of carbon monoxide from measurements of pollution in the troposphere (MOPITT), Geophys. Res. Lett., 31, L23105, doi:10.1029/2004GL021128, 2004.

Kar, J., Jones, D. B. A., Drummond, J. R., Attie, J. L., Liu, J., Zou, J., Nichitiu, F., Seymour, M. D., Edwards, D. P., Deeter, M. N., Gille, J. C., and Richter, A.: Measurement of low altitude CO over the Indian subcontinent by MOPITT, J. Geophys. Res., 113, D16307, doi;10.1029/2007JD009362, 2008.

Kar, J., Jones, D. B. A., and Drummond, J. R.: Comment on "Seasonal distribution of ozone and its precursors over the tropical Indian region using regional chemistry-transport model", by Sompriti Roy et al., J. Geophys. Res., 114, D19303, doi:10.1029/2009JD011742, 2009.

Lawrence, M. G., Rasch, P. J., von Kuhlmann, R., Williams, J., Fischer, H., de Reus, M., Lelieveld, J., Crutzen, P. J., Schultz, M., Stier, P., Huntrieser, H., Heland, J., Stohl, A., Forster, C., Elbern, H., Jakobs, H., and Dickerson, R. R.: Global chemical weather forecasts for field campaign planning: predictions and observations of large-scale features during MINOS, CONTRACE, and INDOEX, Atmos. Chem. Phys., 3, 267–289, doi:10.5194/acp-3-267-2003, 2003.

Lawrence, M. G. and Lelieveld, J.: Atmospheric pollutant outflow from southern Asia: a review, Atmos. Chem. Phys. Discuss., 10, 9463–9646, doi:10.5194/acpd-10-9463-2010, 2010.

Li., Q., Jiang, J. H., Wu, D. L., Read, W. G., Livesey, N. J., Waters, J. W., Zhang, Y., Wang, B., Filipiak, M. J., Davis, C. P., Turquety, S., Wu. S., Park, R. J., Yantosca, R. M., and Jacob, D. J.: Convective outflow of south Asian pollution: a global CTM simulation compared with EOS MLS observations, Geophys. Res. Lett., 32, L14826, doi;10.1029/2005GL022762, 2005.

Liu, Z., Liu, D., Huang, J., Vaughan, M., Uno, I., Sugimoto, N., Kittaka, C., Trepte, C., Wang, Z., Hostetler, C., and Winker, D.: Airborne dust distributions over the Tibetan Plateau and surrounding areas derived from the first year of CALIPSO lidar observations, Atmos. Chem. Phys., 8, 5045–5060, doi:10.5194/acp-8-5045-2008, 2008.

Liu, Z., Vaughan, M. A., Winker, D. M., Kittaka, C., Kuehn, R. E., Getzewich, B. J., Trepte, C. R., and Hostetler, C. A.: The CALIPSO Lidar Cloud and Aerosol Discrimination: Version 2 Algorithm and Initial Assessment of Performance, J. Atmos. Oceanic Technol., 26, 1198–

1213, doi:10.1175/2009JTECHA1229.1, 2009.
Liu, Z., Kuehn, R., Vaughan, M., Winker, D., Omar, A., Powell, K., Trepte, C., Hu, Y., and Hostetler, C.: The CALIPSO Cloud And Aerosol Discrimination: Version 3 Algorithm and Test Results, 25th International Laser Radar Conference (ILRC), St. Petersburg, Russia, (available at: http://www-calipso.larc.nasa.gov/resources/pdfs/ILRC_LaRC_2010/Liu_ILRC25_2010.pdf), 2010.
Omar, A. H., Winker, D. M., Kittaka, C., Vaughan, M. A., Liu, Z., Hu, Y., Trepte, C. R., Rogers, R. R., Ferrare, R. A., Lee, K.-P., Kuehn, R., and Hostetler, C. A.: The CALIPSO automated aerosol classification and lidar ratio selection algorithm, J. Atmos. Ocean. Technol., 26, 1994–2014, 2009.
Park, M., Randel, W. J., Gettelman, A., Massie, S. T., and Jiang, J. H.: Transport above the Asian summer monsoon anticyclone inferred from Aura Microwave Limb Sounder tracers, J. Geophys. Res., 112, D16309, doi:10.1029/2006JD008294, 2007.
Roy, S., Beig. G., and Jacob, D.: Seasonal distribution of ozone and its precursors over the tropical Indian region using regional chemistry-transport model, J. Geophys. Res., 113, D21307, doi:10.1029/2007JD009712, 2008.
Tripathi, S. N., Tare, V., Chinnam, N., Srivastava, A. K., Dey, S., Agarwal, A., Kishore, S., Lal, R. B., Manar, M., Kanawade, V. P., Chauhan, S. S. S., Sharma, M., Reddy, R. R., Rama Gopal, K., Narasimhulu, K., Reddy, L. S. S., Gupta, S., and Lal, S.: Measurements of atmospheric parameters during Indian Space Research Organization Geosphere Biosphere Programme Land Campaign II at a typical location in the Ganga basin: 1. Physical and optical properties, J. Geophys. Res., 111, D23209, doi:10.1029/2006JD007278, 2006.
Vaughan, M., Kuehn, R., Tackett, J., Rogers, R., Liu, Z., Omar, A., Getzewich, B., Powell, K., Hu, Y., Young, S., Avery, M., Winker, D., and Trepte, C.: Strategies for Improved CALIPSO Aerosol Optical Depth Estimates, 25th International Laser Radar Conference (ILRC), St. Petersburg, Russia, (available at: http://www-calipso.larc.nasa.gov/resources/pdfs/ILRC_LaRC_2010/Vaughan_ILRC25_2010.pdf), 2010.
Winker, D. M., Vaughan, M. A., Omar, A., Hu, Y., Powell, K. A., Liu, Z., Hunt, W. H., and Young, S. A.: Overview of the CALIPSO mission and CALIOP data processing algorithms, J. Atmos. Ocean. Tech., 26, 2310–2322, 2009.
Xiong, X., Houweling, S., Wei, J., Maddy, E., Sun, F., and Barnet, C.: Methane plume over south Asia during the monsoon season: satellite observation and model simulation, Atmos. Chem. Phys., 9, 783–794, doi:10.5194/acp-9-783-2009, 2009.

ACPD
10, 20887–20920, 2010

The Bihar Pollution Pool as observed from MOPITT, CALIPSO and TOR

J. Kar et al.

Ziemke, J. R., Chandra, S., Duncan, B. N., Froidevaux, L., Bhartia, P. K., Levelt, P. F., and Waters, J. W.: Tropospheric ozone determined from Aura OMI and MLS: Evaluation of measurements and comparison with the Global Modeling Initiative's Chemical Transport Model, J. Geophys. Res., 111, D19303, doi:10.1029/2006JD007089, 2006.

ACPD

10, 20887–20920, 2010

The Bihar Pollution Pool as observed from MOPITT, CALIPSO and TOR

J. Kar et al.

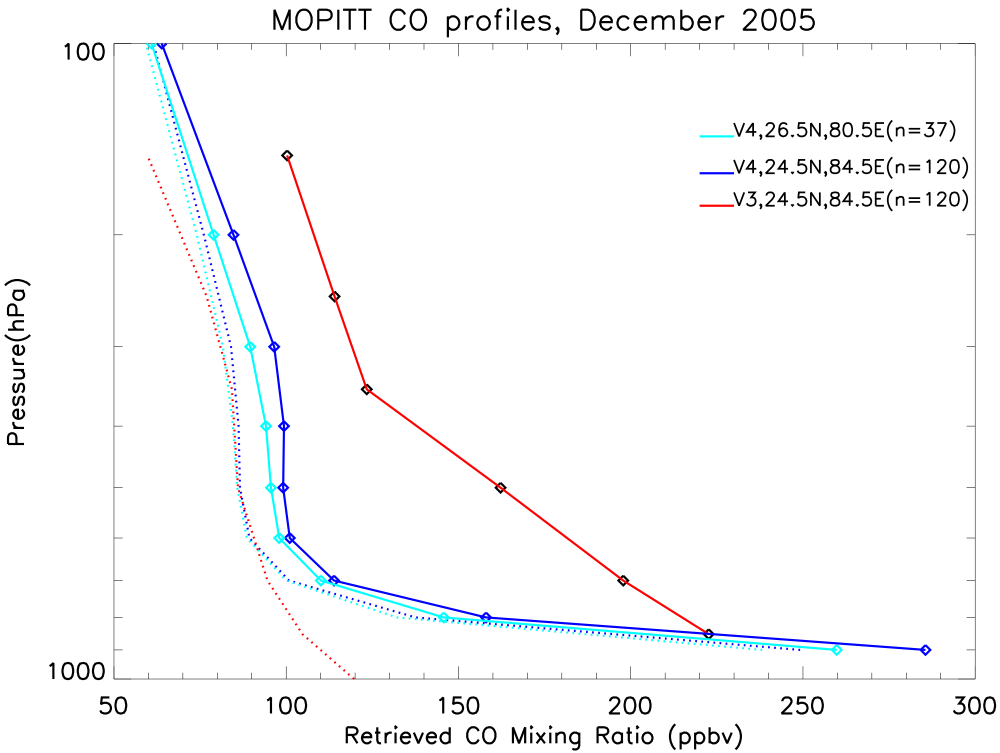

Fig. 1. MOPITT CO profiles at two locations over the Indo-Gangetic basin (level 3 monthly mean gridded data). Note that there were no corresponding profiles within the grid cell centered at 26.5° N, 80.5° E in version 3 of MOPITT data. The dashed curves are the corresponding a priori profiles used in the CO retrievals. The number of profiles for each grid cell is shown in brackets.

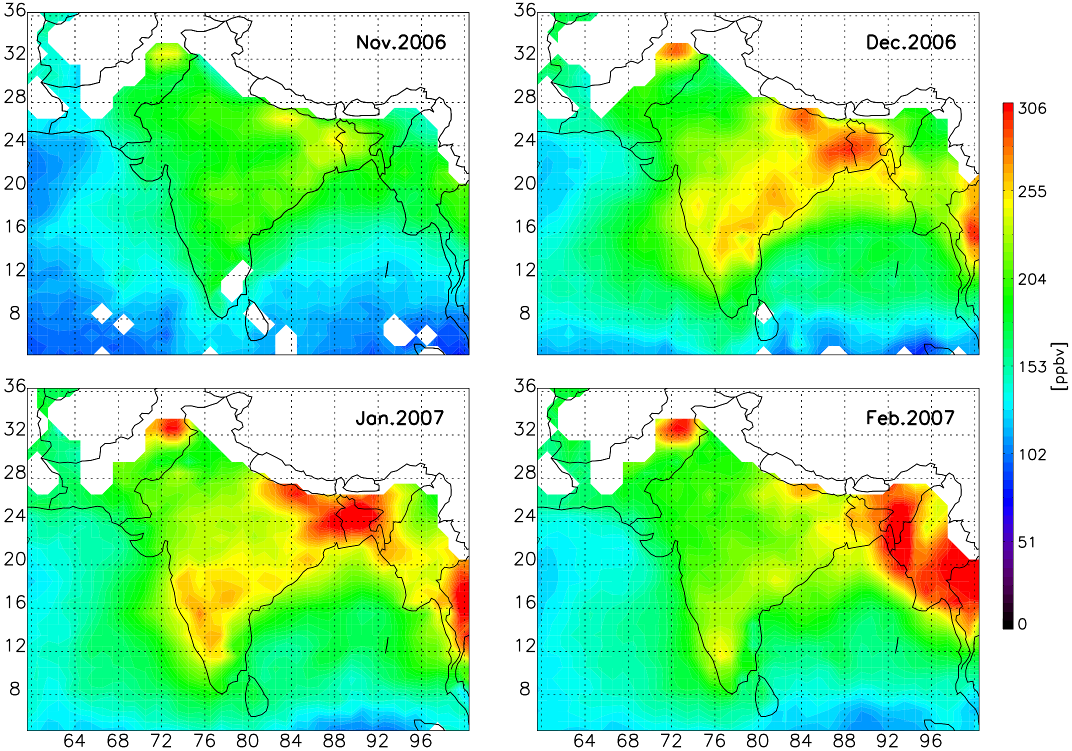

Fig. 2. Evolution of the Bihar Pollution Pool in MOPITT CO retrievals (version 4, level 3) at 900 hPa level. Only the dayside data with mean uncertainty less than 50% have been used for these plots.

ACPD
10, 20887–20920, 2010

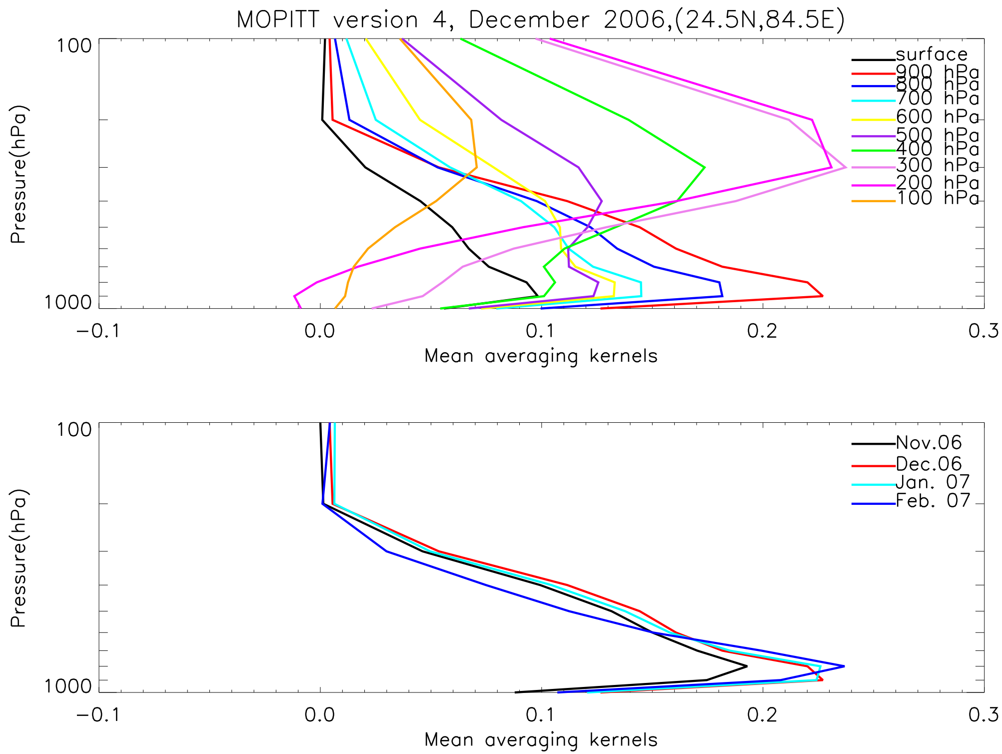

Fig. 3. (a) Monthly mean averaging kernels from version 4 MOPITT data at 24.5° N, 84.5° E for December 2006 and **(b)** Monthly mean averaging kernels at 900 hPa for November 2006 through February 2007 at the same location.

ACPD
10, 20887–20920, 2010

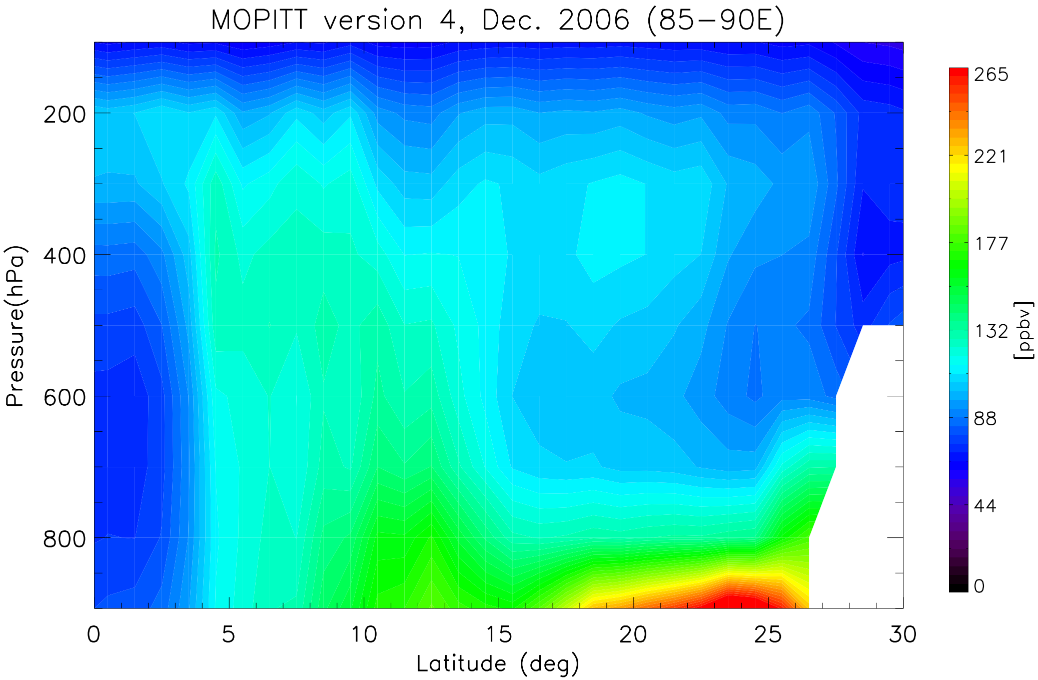

Fig. 4a. Pressure-Latitude cross section of CO mixing ratios retrieved from MOPITT version 4 along 85° E–90° E.

ACPD
10, 20887–20920, 2010

The Bihar Pollution Pool as observed from MOPITT, CALIPSO and TOR

J. Kar et al.

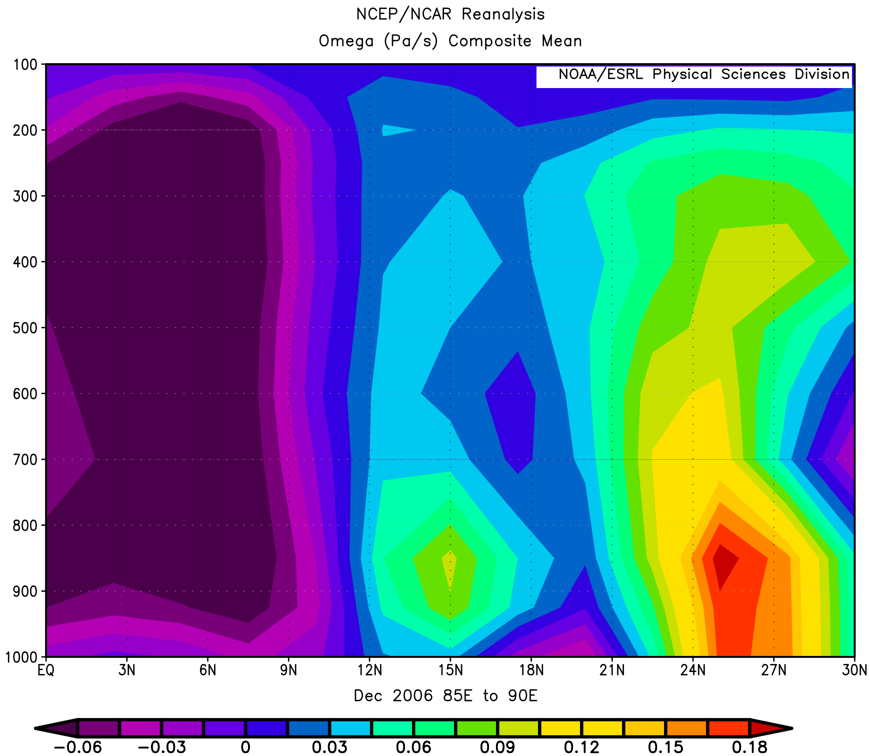

Fig. 4b. Pressure latitude cross section of omega (Pa/s) along 85° E–90° E from NCEP reanalyses for December 2006. Image provided by the NOAA/ESRL Physical Sciences Division, Boulder Colorado from their Web site at http://www.esrl.noaa.gov/psd/.

ACPD
10, 20887–20920, 2010

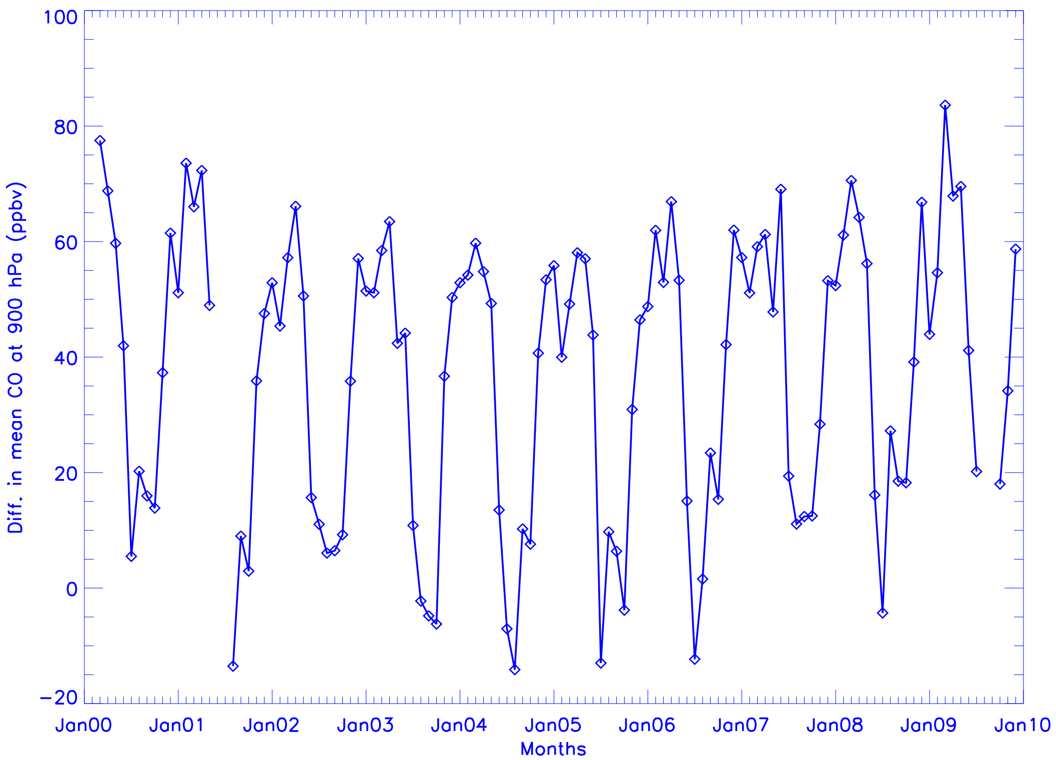

Fig. 5. Time series of the difference in mean CO at 900 hPa between the BPP area (20° N–27° N, 80°–90° E) and western India (20° N–27° N, 65° E–80° E).

ACPD
10, 20887–20920, 2010

The Bihar Pollution Pool as observed from MOPITT, CALIPSO and TOR

J. Kar et al.

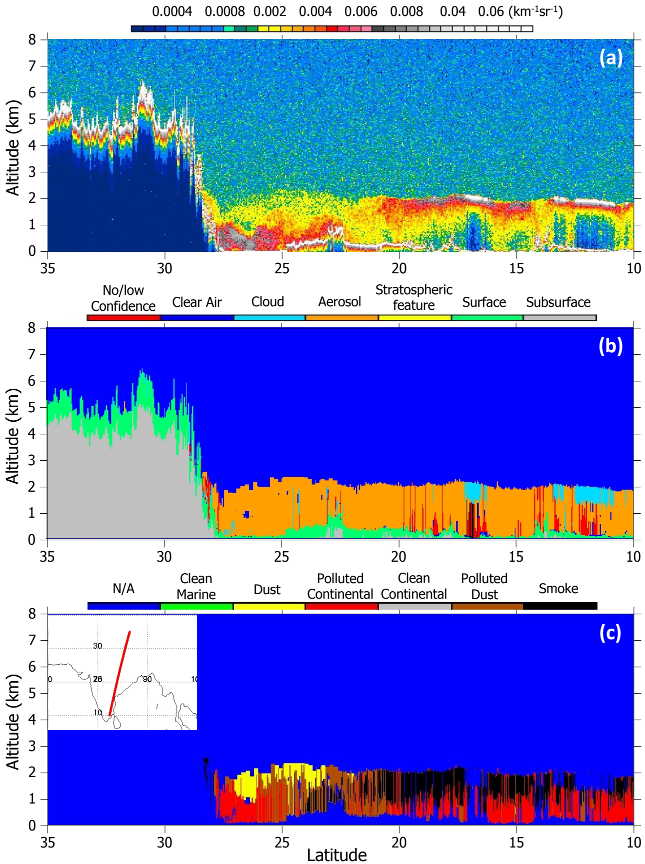

Fig. 6. (a) Total attenuated backscatter at 532 nm, **(b)** the vertical feature mask and **(c)** the aerosol subtypes from CALIPSO (version 3.01 data) on 1 January 2007 along a transect crossing the Bihar pollution pool showing the low altitude aerosols over this area. The transect is shown in the inset of the bottom panel.

ACPD
10, 20887–20920, 2010

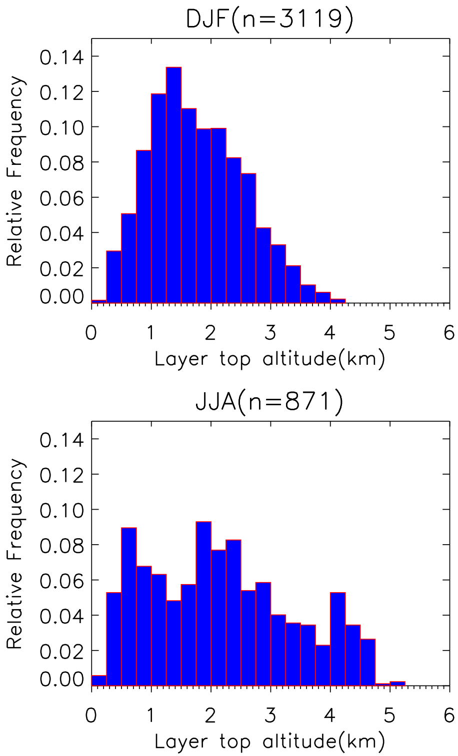

Fig. 7. Altitude of aerosol layer tops (above the surface) from CALIPSO over the BPP area in December 2006–February 2007. Only night time data with CAD scores of −100 were used.

ACPD
10, 20887–20920, 2010

The Bihar Pollution Pool as observed from MOPITT, CALIPSO and TOR

J. Kar et al.

Title Page
Abstract | Introduction
Conclusions | References
Tables | Figures
◂| |▸
◂ ▸
Back | Close
Full Screen / Esc
Printer-friendly Version
Interactive Discussion

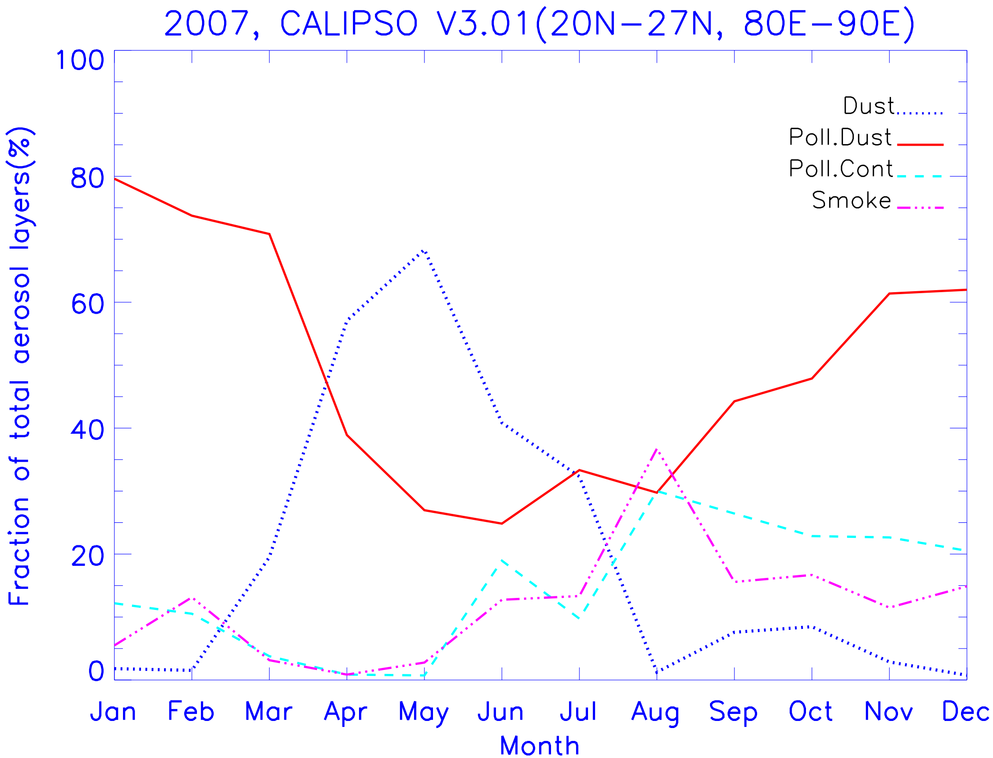

Fig. 8. Seasonal variation of the major aerosol subtypes over BPP as a fraction of the total number of aerosol layers. All night time aerosol layers with CAD scores of −100 and having layer tops less than 6 km above ground were used.

ACPD
10, 20887–20920, 2010

The Bihar Pollution Pool as observed from MOPITT, CALIPSO and TOR

J. Kar et al.

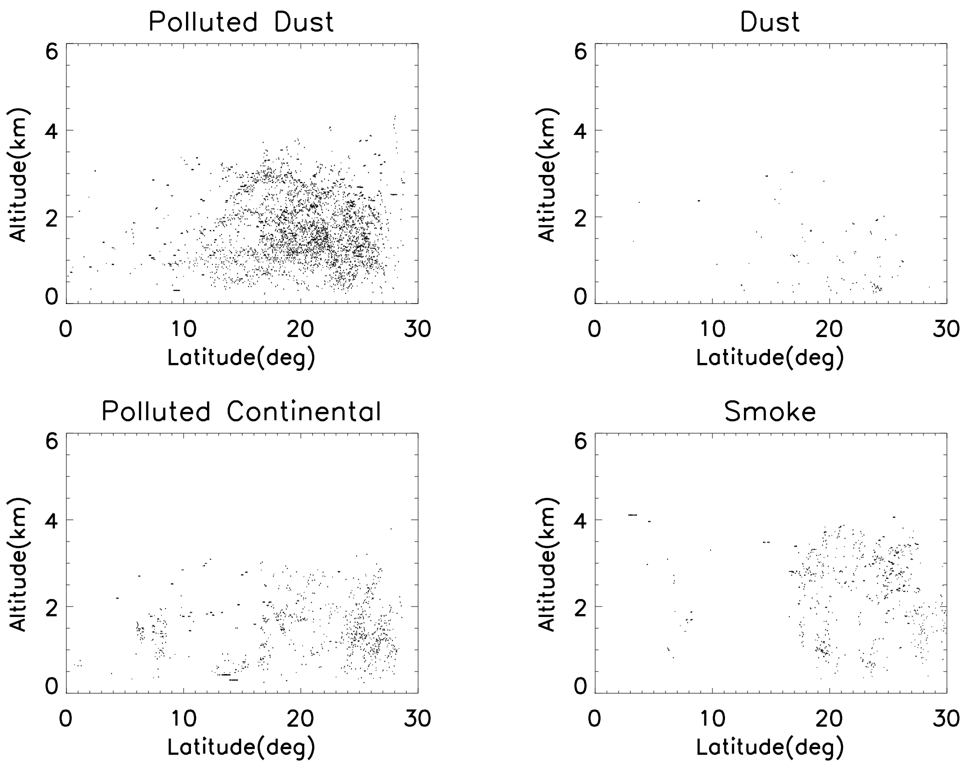

Fig. 9. Altitude distribution of the layers of dominant aerosol subtypes along 80° E–90° E between December 2006 and February 2007. Altitudes refer to top of the layers above the surface.

ACPD
10, 20887–20920, 2010

The Bihar Pollution Pool as observed from MOPITT, CALIPSO and TOR

J. Kar et al.

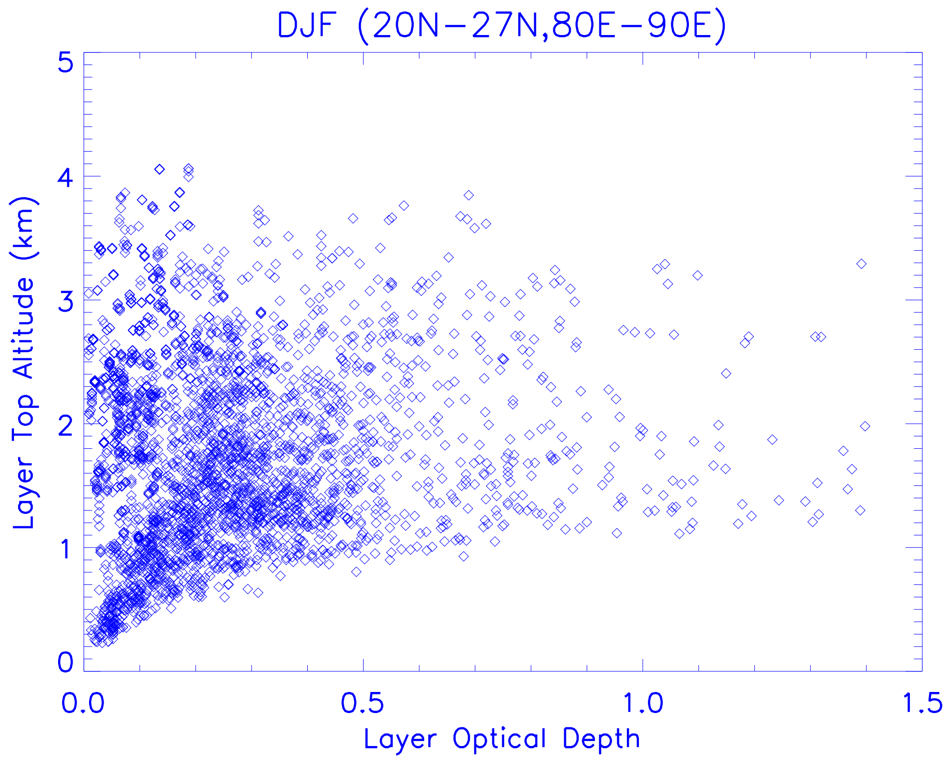

Fig. 10. Layer optical depths (532 nm) over the BPP area during the winter of 2006–2007. Only the layers with CAD scores of −100 and extinction QC value of 0 or 1 were used.

ACPD
10, 20887–20920, 2010

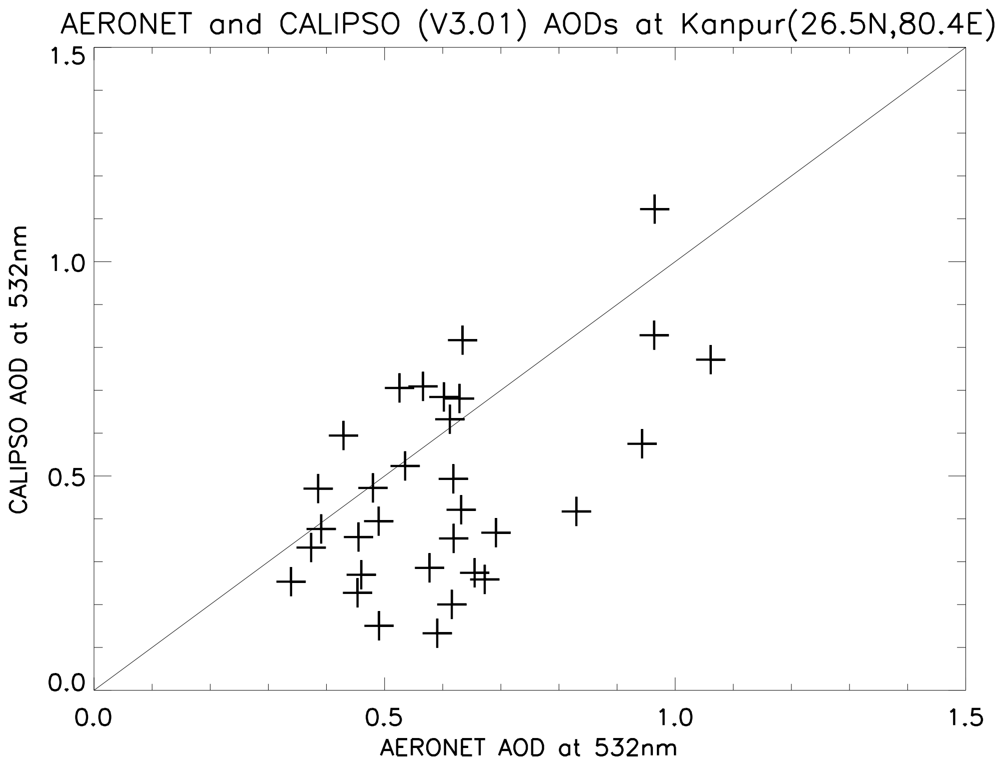

Fig. 11. Comparison of monthly mean column AODs from CALIPSO (version 3) and AERONET station at Kanpur (level 2 version 2 data) near the BPP area. All daytime data between June 2006 and December 2009 from CALIPSO were used.

ACPD
10, 20887–20920, 2010

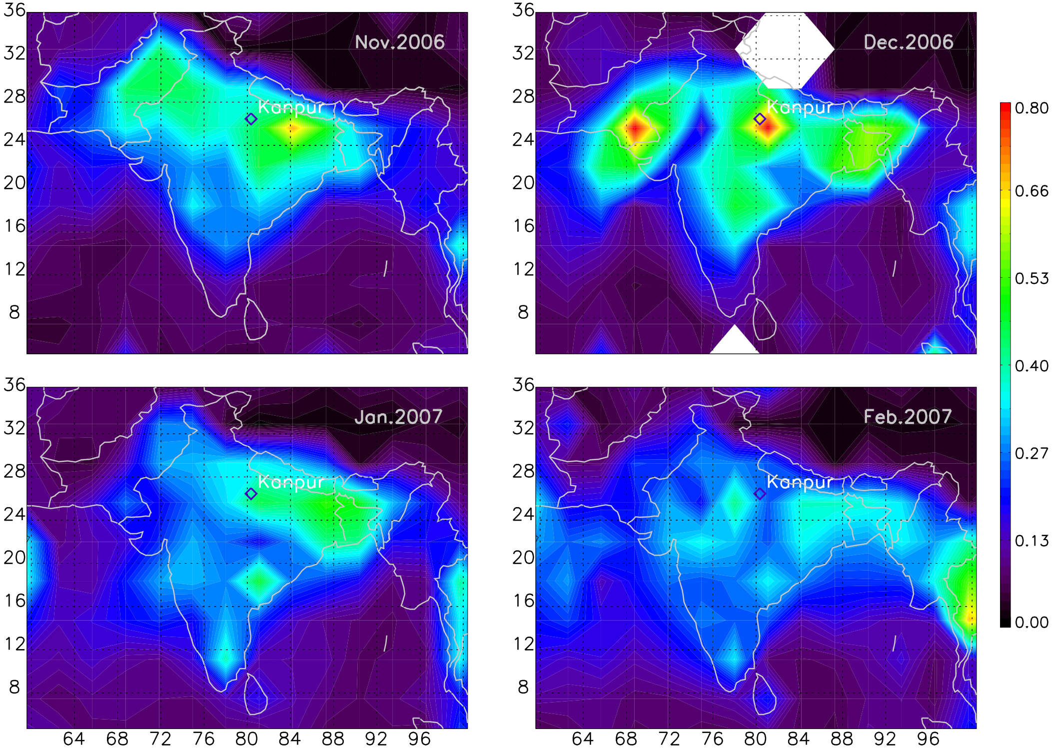

Fig. 12. Column AOD at 532 nm over the BPP area retrieved by CALIPSO version 3 between November 2006 and February 2007. Night time data with extinction QC value of 0 or 1 in each of the layers in the column were used.

ACPD
10, 20887–20920, 2010

The Bihar Pollution Pool as observed from MOPITT, CALIPSO and TOR

J. Kar et al.

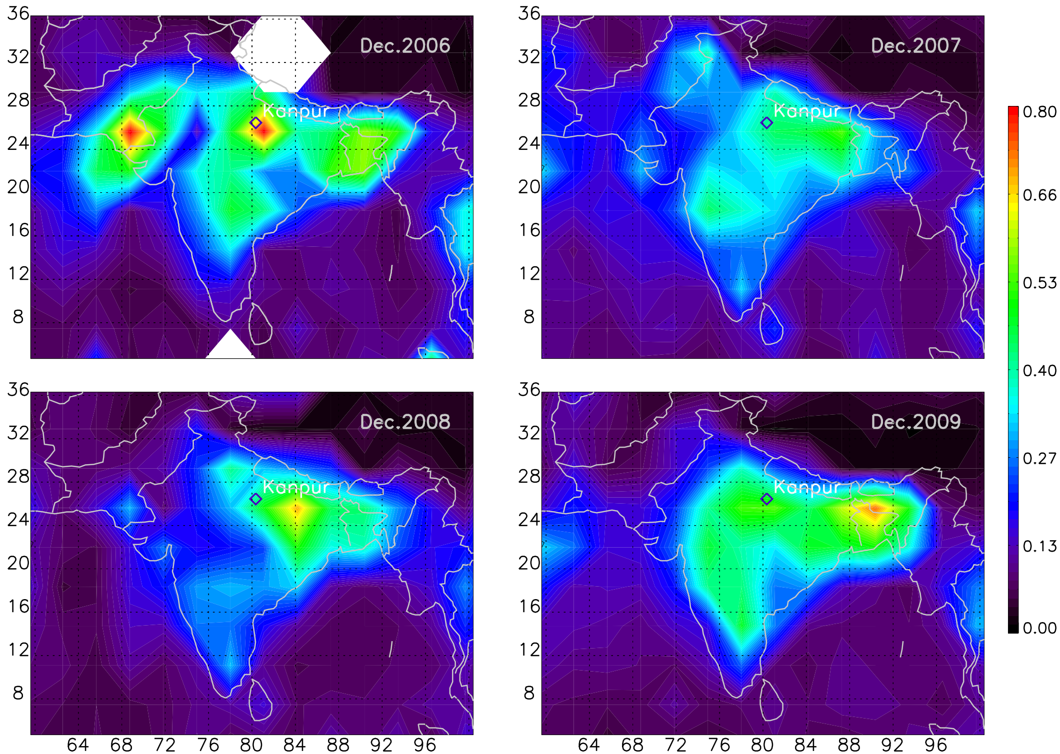

Fig. 13. Inter annual variability in AOD at 532 nm from CALIPSO over the BPP area for December for night time aerosols.

ACPD
10, 20887–20920, 2010

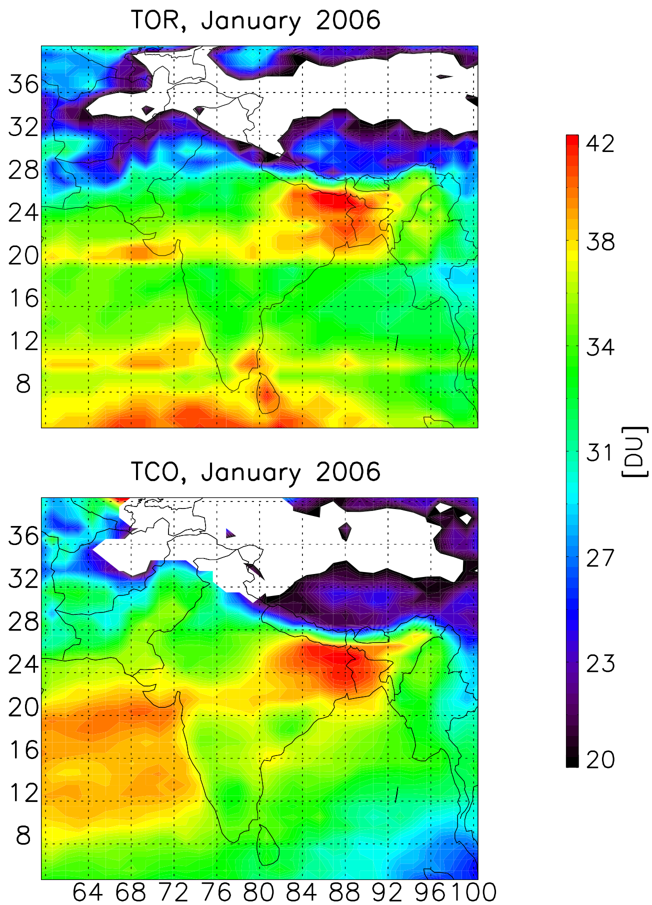

Fig. 14. Distribution of the tropospheric ozone column from TOR (top panel) and TCO (bottom panel) for January 2006.

ACPD
10, 20887–20920, 2010

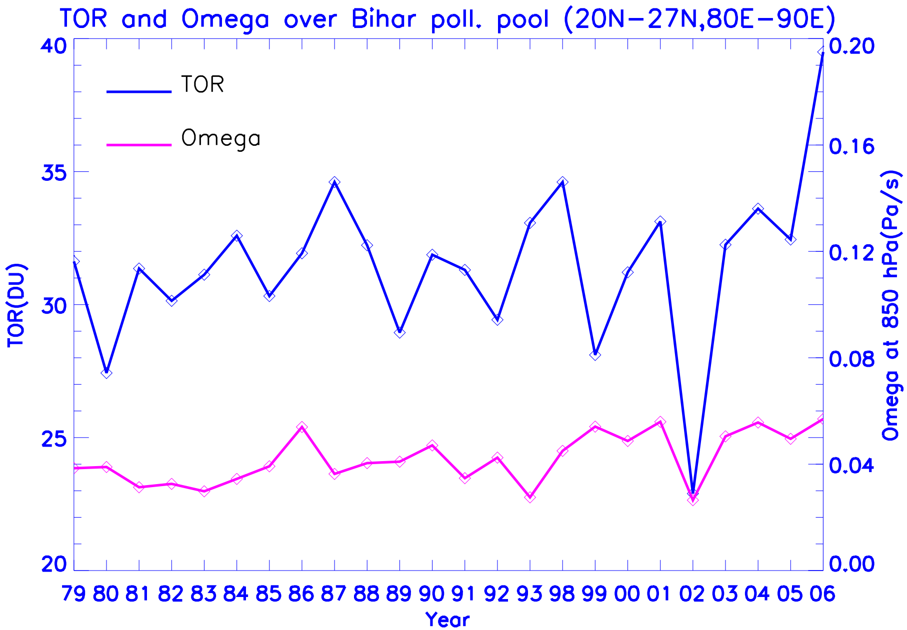

Fig. 15. TOR in January over the BPP area from 1979–2006 and the corresponding pressure tendency (omega, from the NCEP reanalyses). Positive values of omega indicate subsidence over the area for all years. Note that TOR data are not available from 1994 to 1997.

ACPD
10, 20887–20920, 2010